Application of a Semi-Automatic Cartilage Segmentation Method for Biomechanical Modeling of the Knee Joint

Mimmi K. Liukkonen[1,2], Mika E. Mononen[1], Petri Tanska[1], Simo Saarakkala[3,4,5], Miika T. Nieminen[3,4,5], and Rami K. Korhonen[1,2]

[1]*Department of Applied Physics, University of Eastern Finland, Kuopio, Finland*

[2]*Diagnostic Imaging Centre, Kuopio University Hospital, Kuopio, Finland*

[3]*Research Unit of Medical Imaging, Physics and Technology, University of Oulu, Oulu, Finland*

[4]*Medical Research Center Oulu, University of Oulu, Oulu, Finland*

[5]*Department of Diagnostic Radiology, Oulu University Hospital, Oulu, Finland*

M. K. Liukkonen (e-mail: mimmi.liukkonen@uef.fi)

Application of a Semi-Automatic Cartilage Segmentation Method for Biomechanical Modeling of the Knee Joint

Manual segmentation of articular cartilage from knee joint 3D magnetic resonance images (MRI) is a time consuming and laborious task. Thus, automatic methods are needed for faster and reproducible segmentations. In the present study, we developed a semi-automatic segmentation method based on radial intensity profiles to generate 3D geometries of knee joint cartilage which were then used in computational biomechanical models of the knee joint. Six healthy volunteers were imaged with a 3T MRI device and their knee cartilages were segmented both manually and semi-automatically. The values of cartilage thicknesses and volumes produced by these two methods were compared. Furthermore, the influences of possible geometrical differences on cartilage stresses and strains in the knee were evaluated with finite element modeling. The semi-automatic segmentation and 3D geometry construction of one knee joint (menisci, femoral and tibial cartilages) was approximately two times faster than with manual segmentation. Differences in cartilage thicknesses, volumes, contact pressures, stresses, and strains between segmentation methods in femoral and tibial cartilage were mostly insignificant ($p > 0.05$) and random, i.e., there were no systematic differences between the methods. In conclusion, the devised semi-automatic segmentation method is a quick and accurate way to determine cartilage geometries; it may become a valuable tool for biomechanical modeling applications with large patient groups.

Keywords: Cartilage, Finite Element Analysis, Image Segmentation, Knee, Magnetic Resonance Imaging

Introduction

Finite element (FE) modeling can be used as a non-invasive method to evaluate stresses, strains and contact mechanics within the knee joint subjected to various loading conditions, providing parameters which cannot be obtained from imaging. In order to generate subject-specific geometries for incorporation into biomechanical knee joint models, it is necessary to have accurate segmentation of tissues from medical images (Anderson et al. 2010). Especially in biomechanical modeling, manual segmentation is currently the most common approach used for knee joint cartilage segmentation from magnetic resonance (MR) images (Kwon et al. 2014; Mononen et al. 2016; Ali et al. 2017). However, it is time consuming, laborious, and suffers from intra- and inter-observer variability (Shim et al. 2009), which limits the use of computational modeling in larger patient groups. Therefore, it would be advantageous if there were accurate, automatic or semi-automatic segmentation methods.

Automatic segmentation of knee joint cartilages from MRI is a challenging task due to lack of contrast between cartilage and other soft tissues, MR artefacts, and noise. Semi-automatic and automatic segmentation methods have been developed to measure the thickness and volume of healthy and osteoarthritic articular cartilage (Folkesson et al. 2007; Fripp et al. 2007; Velut et al. 2008; Dodin et al. 2010; Tamez-Peña et al. 2012; Shan et al. 2014). However, those have not been developed or applied to estimate the 3D geometry in biomechanical knee joint models. Baldwin et al. (2010) introduced a semi-automatic statistical shape model based segmentation method for subject-specific FE modeling. The weakness of this method was that it still required manually segmented training sets.

Even though different algorithms have been developed for knee joint cartilage segmentation (Folkesson et al. 2007; Velut et al. 2008; Dodin et al. 2010; Tamez-Peña et al. 2012; Shan et al. 2014), there is a need for reproducible and applicable

segmentation methods suitable for computational modeling. Currently, there are no studies which have evaluated the accuracy of knee cartilage segmentation (manual vs. automatic) on the simulated stresses and strains within the knee joint. Therefore, the aim of the current study was to devise a radial intensity based semi-automatic segmentation method for biomechanical modeling purposes. Since the manual segmentation is usually considered as a standard segmentation procedure, it was considered as the reference method. Validation of the presented method (model result from manually and semi-automatically segmented joints) was conducted within healthy knee joints without cartilage lesions or indication of knee OA. We hypothesized that the values obtained with the model results with semi-automatically segmented cartilage layers would be similar to those acquired with manually segmented knee joints.

Methods

Radial intensity based semi-automatic segmentation method

The semi-automatic segmentation method was designed in Matlab (Mathworks Inc., Natick, MA, USA) and applied for the femoral and tibial cartilage. The main goal of the radial intensity segmentation method is to detect cartilage surface and cartilage-bone interface from the radial intensity profiles of the cartilage based on the information available in the clinical MRI.

First, a reference point (RP) from the central point of bone (tibia and femur) and edge points (EP's) of cartilage were selected from a sagittal slice of the knee MR image (an example can be seen from Figure 1a). Subsequently, intensity profiles were calculated between the end points of cartilage at intervals of five degrees (Figure 1a), while the reference point was used as the origin (first intensity value in the intensity profile). Finally, central points of cartilage (peak intensity), cartilage surface and

cartilage-bone interface were determined from intensity profiles using thresholds (Figure 1b).

[Figure1 near here]

The semi-automatic segmentation script worked as follows: The first intensity peak after bone was defined as the central point of cartilage (Figure 1b). Cartilage surface and cartilage-bone interface were then calculated using the obtained central point of the cartilage and shape of the intensity profile. Starting from the central point of the cartilage (peak intensity), the pixel number along with the intensity profile path was increased or decreased one by one as long as the threshold value was exceeded and the difference between the intensity values of two consecutive pixels in the descending parts of the profile (either toward bone or cartilage surface) was positive or zero. The threshold was set to ~45% and ~60% of the maximum intensity (after subtracting the intensity from bone) for tibial and femoral cartilage, respectively (Figure 1b). Threshold values were different because the intensities in femoral and tibial cartilage as well as in femur and tibia bones were not equal.

The same procedure as described in the previous paragraph was repeated for every intensity profile resulting in a series of point pairs along the cartilage surface and cartilage-bone interface (Figure 1c). Finally, the detected points were joined together and masks were produced using the Matlab *"roipoly"*-function (Figure 1d). Occasionally, there was noise or inadequate contrast between cartilage and other tissues, resulting in incorrect segmentation points. Those points were corrected (by visual inspection) manually by moving the incorrect points to the correct position. In addition, the pixels overlapping between tibial and femoral cartilages were removed. This segmentation procedure described above was repeated with all MRI slices.

Imaging and segmentation

Six knee joints from healthy volunteers were imaged with a clinical 3T MRI scanner (Philips Achieva, Philips Medical Systems, Best, Netherlands or Magnetom Skyra, Siemens Healthcare, Erlangen, Germany) (Figure. 2a, Table 1). The following imaging sequences were used: 3D Proton Density Turbo Spin-Echo Spectral Attenuated Inversion Recovery (3D PD TSE SPAIR: TR = 1300 ms, TE = 32.3 ms, Flip Angle = 90º, Spatial resolution = 0.5 mm, and Slice Thickness = 0.5 mm), 3D Proton Density Fast Spin-Echo with Fat Saturation (3D PD FSE FS: TR = 1200 ms, TE = 26 ms, Flip Angle = 120º, Spatial resolution = 0.6 mm, and Slice Thickness = 0.6 mm), or 3D T2-weighted Gradient Echo (3D T2 GE: TR = 14.1 ms, TE = 5 ms, Flip Angle = 25º, Spatial resolution = 0.6 mm, and Slice Thickness = 0.6 mm). The study was conducted with permissions from the ethical committees of Kuopio University Hospital, Kuopio, Finland and Oulu University Hospital, Oulu, Finland. Written consent was obtained from all study subjects.

[Figure2 near here] [Table1 near here]

After MRI, cartilages were segmented manually using Mimics v15.01 (Materialise, Leuven, Belgium) and semi-automatically using Matlab v7.14.0 (Mathworks Inc., Natick, MA, USA) (Figure. 2b). Manual segmentation was conducted by a physicist who has also radiographer's professional competence and clinical experience on evaluating knee joint MR images. Semi-automatic segmentation was conducted twice to test intra-observer repeatability. Menisci were segmented manually using Mimics, and the same menisci were used in the corresponding semi-automatically segmented knee joint models (see below) in order to minimize the number of variables. Finally, 3D geometries were constructed from manually and semi-automatically segmented cartilages and menisci using Mimics (Figure. 2c).

FE analysis

Using Abaqus v6.13-3 (Dassault Systèmes, Providence, RI, USA), manually and semi-automatically segmented 3D knee geometries were meshed using second-order, 10-node modified tetrahedral elements (type C3D10M) (Figure 2d). Tetrahedral elements were chosen since they provide a more straightforward mesh generation which is needed in modeling applications with a large number of patients. Modified elements were used because of their good capabilities in contact modeling. The average element numbers in tibial and femoral cartilage and menisci were 25000, 18000 and 29000, respectively. A mesh sensitivity study was conducted by comparing the model with the tetrahedral mesh to a model with an 8-node continuum hexahedral (type C3D8) mesh since the latter element type has proven capabilities in contact analysis. In this analysis, axial loading was applied similarly as described below and cartilage was modeled as an isotropic elastic and nearly incompressible material (Young's modulus = 15 MPa and Poisson's ratio = 0.475 (Haut Donahue et al. 2003)). Different mesh types produced less than a 5 % difference in the average Von Mises stresses (Figure 3). Thus, the tetrahedral mesh was assumed to be adequate for the remainder of the simulations.

[Figure3 near here] [Table2 near here]

Cartilages and menisci were modeled as transversely isotropic elastic materials. Material parameters (Table 2) for cartilages and menisci were taken from the literature (Goertzen et al. 1997; Shepherd and Seedhom 1999; Elliott et al. 2002; Korhonen et al. 2002; Mow et al. 2005; Vaziri et al. 2008; Danso et al. 2015). This material model was chosen, instead of a more sophisticated alternative (such as a fibril reinforced poro(visco)elastic material (Li et al. 2000; Wilson et al. 2004; García and Cortés 2007; Halonen et al. 2013), because it speeds up the model generation process and simulation times. Rapid model generation is important when utilizing this kind of modeling in

clinical applications and follow-up of patients. Moreover, a previous study suggested that the instantaneous response of the elastic material is the same with a poroelastic material in the knee (Garcia et al. 1998) and that the maximum contact pressure could be similar between elastic and poroelastic material models (Li and Gu 2011). Meniscal attachments were modeled using linear springs (type SPRINGA) with the moduli of 226 MPa and 139 MPa for the anterior and posterior meniscal attachments, respectively (Hauch et al. 2010). The plane of isotropy (1-2) was set parallel to the cartilage surface, while in the menisci, directions 1, 2 and 3 were radial, axial and circumferential directions, respectively (Figure 2d).

Femur and tibia bones were considered as rigid. The bottom surface of the femoral cartilage, which represents the femoral cartilage-bone interface, was fixed to a reference point using a coupling constraint method in Abaqus. The reference point was located in the middle point between lateral and medial epicondyles of the femur (Mononen et al. 2013) (Figure 2d). The bottom nodes of tibial cartilage representing the cartilage-bone interface were fixed in all directions. Free varus-valgus rotation around the reference point was allowed to ensure good contact between the femoral and tibial cartilages (Mononen et al. 2013), while other degrees of freedom were fixed. Hard surface-to-surface contacts with frictionless sliding and penalty contact enforcement were applied between the cartilage-cartilage and cartilage-meniscus interfaces. The simulation was performed in two separate steps. During the first step, femoral cartilage was moved along with the axial direction (y-axis) to the contact with tibial cartilage. In the second step, 1000 N axial loading was applied on the reference point within 0.1 s (Figure 2d). Similarly as with the segmentation and material choice, this loading (instead of a more complex alternative, such as walking) was applied since it can be implemented easily and quickly and our aim was to investigate the importance of the

model geometry on the results (not site- and time-specific cartilage responses). Thus, we assumed here that the conclusions would be the same with more complex loading.

Analyzed parameters and statistics

We compared the volumes and thicknesses of femoral and tibial cartilages, and the total segmentation time required for knee joint cartilages between different segmentation methods. Furthermore, contact pressures, stresses and compressive strains from the contact areas of femoral and tibial cartilages between the models with different segmentation methods were compared. Statistical comparisons between semi-automatic and manual segmentation methods were conducted using Wilcoxon signed-rank test and the level of statistical significance was set at 0.05 (SPSS v. 21, SPSS Inc., Chicago, IL). Dice similarity coefficients (DSC) were calculated between manual and semi-automatic segmentations and between two semi-automatic segmentations to study the similarity of two different segmentations as follows: $DSC = 2J/(1+J)$, where $J = (A \cap B)/(A \cup B)$ and A and B are the two different segmentations (Pedoia et al. 2016). Intra-observer repeatability was tested using Intraclass Correlation Coefficient (ICC).

Results

The average number of segmented slices was 129 (range 114-156). The average time for semi-automatic segmentation and 3D geometry construction of one knee joint was approximately 4 hours. In contrast, it took at least 8 hours to segment and construct 3D geometries from tibial and femoral cartilages using the manual “pixel by pixel” segmentation method.

The semi-automatic segmentation method showed excellent intra-observer repeatability in the femoral and tibial cartilage volumes (ICC 0.989 and 0.965,

respectively). The mean differences in the femoral and tibial cartilage volumes between the repeated semi-automatic segmentations were 1.9% and 3.0%, respectively. Moreover, DSC values for the femoral and tibial cartilages were 0.76 ± 0.12 and 0.76 ± 0.12, respectively.

Average differences in the cartilage volumes between manual and semi-automatic segmentation methods were 0.68 ± 0.80 cm^3, 0.12 ± 0.17 cm^3 and 0.04 ± 0.33 cm^3 for the femoral, lateral tibial and medial tibial cartilages, respectively; these differences were statistically insignificant ($p > 0.05$, Figure 4a). Average differences in the cartilage thicknesses between manually and semi-automatically segmented cartilages were 0.2 ± 0.3 mm, 0.2 ± 0.2 mm, 0.1 ± 0.3 mm and 0.2 ± 0.2 mm for the lateral femoral, medial femoral, lateral tibial and medial tibial cartilages, respectively. There were no systematic differences in the determined cartilage thicknesses between these two segmentation methods, *i.e.*, neither method resulted in either systematically greater or lower values (Figure 4b). The only statistically significant difference in thickness between the methods was observed in the medial tibial cartilage ($p < 0.05$). Moreover, DSC values between manually and semi-automatically segmented femoral and tibial cartilages were 0.86 ± 0.02 and 0.88 ± 0.01, respectively.

[Figure4 near here]

The contact areas in the models with semi-automatically segmented geometries were detected at the same location as in the models with manually segmented geometries (Figure. 5a). Differences in the contact pressures and stress distributions between the models were random, *i.e.*, the locations of the highest values were not dependent on the segmentation method (Figures. 5a, 5b and Figure 1 in Supplementary material).

[Figure5 near here]

Differences in the peak contact pressures, Von Mises stresses and compressive strains between semi-automatically and manually segmented models were random and not significantly different (Figure 6). Average differences in the peak contact pressures between semi-automatically and manually segmented cartilages were 1.0 ± 1.6, 0.7 ± 1.4, 0.04 ± 0.7 and 0.2 ± 1.7 MPa in the lateral femoral, medial femoral, lateral tibial and medial tibial cartilages, respectively. Similarly, average differences in the peak Von Mises stresses between the methods were 0.9 ± 0.9, 0.7 ± 1.1, 0.2 ± 1.3 and 0.5 ± 1.6 MPa and those in the peak compressive strains were 2.5 ± 4.4, 1.0 ± 3.9, 1.8 ± 3.9 and 0.7 ± 5.4 percentage points in the corresponding locations, respectively.

Differences in the mean contact pressures, Von Mises stresses and compressive strains between the methods were also random and mostly insignificant ($p > 0.05$) (Table 3). Average differences between semi-automatically and manually segmented cartilages in the mean contact pressures were 0.2 ± 0.3, 0.04 ± 0.2, 0.4 ± 0.4 and 0.4 ± 0.6 MPa in the lateral femoral, medial femoral, lateral tibial and medial tibial cartilages, respectively. Similarly, average differences in the mean Von Mises stresses between the methods were 0.04 ± 0.4, 0.3 ± 0.4, 0.3 ± 0.4 and 0.2 ± 0.7 MPa and those in the mean compressive strains were 0.5 ± 2.0, 0.3 ± 1.2, 0.4 ± 2.1 and 1.9 ± 1.4 percentage points in the corresponding locations, respectively.

[Figure6 near here] [Table3 near here]

Discussion

The objective of this study was to verify the applicability of a semi-automatic radial intensity based cartilage segmentation method for biomechanical modeling purposes in orthopaedics. We applied the developed semi-automatic segmentation method in evaluating tibial and femoral cartilage from six healthy subjects. The volumes of

femoral and tibial cartilage produced by the semi-automatic segmentation were comparable to those obtained by the manual segmentation. Furthermore, maximum stresses and strains in the knee joint models acquired with these two segmentation methods were similar.

In clinical practice, automatic or semi-automatic cartilage segmentation methods have been used only for quantifying cartilage volumes and thicknesses in the knee joints (Folkesson et al. 2007; Fripp et al. 2007; Velut et al. 2008; Dodin et al. 2010; Tamez-Peña et al. 2012; Shan et al. 2014). Gan et al. (2014) developed an interactive 2D automatic segmentation method, but in their technique, the segmentation time was three times longer per slice compared to our semi-automatic segmentation method and the final segmentation needed more refinement than our method. As far as we are aware, there exists only one semi-automatic knee cartilage segmentation method (Baldwin et al. 2010) which has been applied for biomechanical modeling purposes. However, that method still required manually segmented training data for segmentation. In contrast, our method is capable of separating knee joint cartilages without training sets which minimizes the amount of manual work.

Verification of the applicability of our semi-automatic segmentation method was performed with six healthy knee joints. Differences in cartilage volumes and thicknesses between segmentation methods were less than 10% (Figure 4a and 4b), which is in a similar reliability range as reported in previous validation studies (Fripp et al. 2007; Dodin et al. 2010; Tamez-Peña et al. 2012). However, those methods did not separate femoral and tibial cartilages into separate regions, they needed previous bone segmentation to the baseline for the cartilage segmentation, or demanded manually segmented training data.

283 The spatial resolution in the MRI images used in this study was 0.5–0.6 mm
284 (~10–20% of the tissue thickness). This means that one pixel difference compared to the
285 manual segmentation can cause over 10 % difference in the cartilage thickness. Due to
286 this fact, our segmentation method was able to replicate manually segmented tissue
287 geometries rather accurately. Furthermore, the average dice similarity coefficient
288 between manual and semi-automatic segmentations was ~0.87, evidence of rather good
289 consistency between the segmentation methods. It is also important to note that the
290 geometrical differences between the segmentation methods were random, *i.e.*, neither
291 method gave systematically higher or lower values. Differences in tissue thicknesses
292 obviously introduce some differences into the simulation results, but that effect was also
293 random between different segmentation methods (Figure 4 and 6, Table 3).

294 In the present study, peak contact pressure values varied between 1.5-7 MPa.
295 Similar values (2-6 MPa) have been reported in previous experimental studies with
296 loading forces of 1000-1200 N (Fukubayashi and Kurosawa 1980; Morimoto et al.
297 2009; Patil et al. 2014). Experimental studies have measured average peak compressive
298 strains of ~17 % and ~15 % in the medial and lateral tibial cartilages, respectively,
299 when subjects were standing in the single fully extended leg position (Carter et al.
300 2015). The average peak cartilage strains simulated in our study were 17.5 % and 13 %
301 in the medial and tibial cartilages, respectively.

302 The average differences in the peak contact pressures between the segmentation
303 methods differed on average by 0.01 MPa, depending on the subject and location.
304 Similarly, average differences in the peak Von Mises stresses and compressive strains
305 were 0.5 MPa and 0.6 percentage points. The largest differences in the peak values were
306 mainly caused by the differences in the cartilage thickness and surface topography.
307 However, all differences in the peak values were statistically insignificant and random,

which indicates that the semi-automatic method did not always produce lower or higher values compared to the manual method.

The average differences in the mean contact pressures, Von Mises stresses and compressive strains between the methods in all locations were less than 0.1 MPa, 0.1 MPa and 0.5 percentage points, respectively, and the direction of the difference was random. The only statistically significant differences between the segmentation methods were seen in the mean contact pressures and compressive strains of the lateral tibial cartilage and those differences were attributable to the small differences in the cartilage thicknesses and surface topography. This altered slightly the contact area affecting the mean values of the analyzed parameters. There were also some inconsistencies between maximum and mean values, i.e., the method which showed a higher maximum value did not always report a higher mean value. This is because the same contact area of manually segmented geometries was used when calculating the results from semi-automatically segmented geometries. Nonetheless, when applying our modeling approach in the evaluation of possible cartilage failure locations (*e.g.*, due to abnormal loading), peak values might be more relevant.

In the present study, the methods (segmentation, mesh generation, material model implementation and loading) were designed so that the knee joint model could be generated and simulated as quickly as possible. This kind of rapid approach (instead of a more complicated but slower technique) would be helpful in clinical applications. Approximately 7 h at minimum was required when segmentation and model generation were accomplished with semi-automatic segmentation, tetrahedral element mesh, transversely isotropic elastic material and axial loading. The simulation time of the working model mentioned above was approximately 3 hours. With manual segmentation, hexahedral elements, fibril reinforced poro(visco)elastic materials and

gait loading (Mononen et al. 2013; Kłodowski et al. 2015), model generation time can easily be close to 1-2 weeks even for an expert in the field. Additionally, the simulation may require over 10 hours' computational time. Moreover, fluent workflow in model generation and simulation necessitates extensive expertise and knowledge in model creation; in fact, the duration of 2 weeks can easily expand to 1 year when the model is very complex. Thus, this simpler and faster model generation and simulation is clearly more suitable for future clinical biomechanical applications with large patient groups, particularly when investigating differences in the values (*e.g.* knee joint mechanics after injury vs. repair).

The tetrahedral mesh could be replaced by a hexahedral mesh which is typically better in contact modeling. However, this would introduce further complexity into the model generation, and based on our tests (Figure 3), the model with the tetrahedral mesh generated a similar result as obtained with the hexahedral mesh. Thus, the tetrahedral mesh was considered feasible for use in our approach. The material models could also be more complex. However, Garcia et al. (1998) showed that the instantaneous response of a transversely isotropic elastic material can be similar to that of a transversely isotropic biphasic material with respect to the indentation geometry. The previous study of Li et al. (2011) showed that the maximum contact pressure could be similar between elastic and poroelastic material models, though the pressure distributions between the models were different. More sophisticated materials would obviously give more information such as fluid pressures and fibril strains, but generating 12 sophisticated knee joint models and converged simulations is a laborious task and not relevant for this kind of comparison study (where we were mostly interested in detecting differences due to knee geometries). We believe this rapid modeling workflow will also be beneficial when predicting the onset and progression of

OA (Gardiner et al. 2016; Mononen et al. 2016) in large patient groups. Simple axial loading could be replaced by subject-specific gait information (Kłodowski et al. 2015) if there were data available (which we did not have). However, this would again introduce more complexity into the model and would slow down both model generation and simulation times. The loading level could also be adjusted patient-specifically. On the other hand, we compared segmentation methods (manual vs. semi-automatic) and the loading was always the same for pair-wise joints, *i.e*. the conclusions would be the same even if we had used subject-specific loading forces.

Our semi-automatic segmentation method is not directly suitable for segmentation of menisci since the signal intensity of the menisci is difficult to separate from other soft tissues by using thresholding, especially in the areas where there is no cartilage-meniscus contact. The creation of intensity profiles from meniscal horns is also complicated due to their shape and size. In addition, we wanted to minimize the number of variables and therefore we used the same manually segmented menisci for the corresponding semi-automatically segmented geometry. One can speculate that with some other MRI sequence and contrast agent, it could be possible to segment the menisci semi-automatically.

Our radial intensity based segmentation method was validated only using healthy volunteers. One might argue about how applicable this method would be for patients with OA. Since the goal of our computational models is to predict subject-specific risks for the onset of OA and even predict the disease progression (Mononen et al. 2016), such as after a knee injury (not yet OA), our use of the segmentation method for healthy cartilage is reasonable.

The validation of the semi-automatic segmentation method was conducted using three different MRI sequences. Cartilage contrast might vary between different

sequences which may affect cartilage thickness and volume. However, this was not a problem with our approach, since the same sequence was segmented manually and semi-automatically, and the statistical comparison was carried out in a pair-wise manner.

Loss of cartilage volume and thickness are related to the progression of OA. However, these changes are typically detected only at a stage where irreversible changes have already occurred. On the other hand, knee cartilage stresses and strains during joint loading could be used as indicators of possible failure points in joints due to abnormal loading (*e.g.*, after joint injury), and might lead to earlier and better diagnostics and treatment planning. The semi-automatic method described in the current study provides accurate quantification of knee cartilage thickness and volume calculations and enables straightforward geometry creation and reliable analysis of stresses and strains in the knee joint. Thus, our semi-automatic segmentation method is a promising advance to allow computational modeling to be conducted in a large number of patients.

Acknowledgements

The research leading to these results has received funding from the Academy of Finland (grant 286526, 305138), Sigrid Juselius Foundation, the strategic funding of the University of Eastern Finland and Kuopio University Hospital (no. 931053), Kuopio University Hospital (VTR grant 5041752), Oulu University Hospital (VTR grant K33745) and Doctoral Programme in Science, Technology and Computing, University of Eastern Finland. CSC – IT Center for Science Ltd, Finland is acknowledged for providing the finite-element modeling software.

References

Ali AA, Harris MD, Shalhoub S, Maletsky LP, Rullkoetter PJ, Shelburne KB. 2017. Combined measurement and modeling of specimen-specific knee mechanics for healthy and ACL-deficient conditions. J. Biomech. 57:117–124. doi:10.1016/j.jbiomech.2017.04.008.

Anderson AE, Ellis BJ, Maas SA, Weiss JA. 2010. Effects of idealized joint geometry

412 on finite element predictions of cartilage contact stresses in the hip. J. Biomech.
413 43:1351–1357. doi:10.1016/j.jbiomech.2010.01.010.
414 Baldwin MA, Langenderfer JE, Rullkoetter PJ, Laz PJ. 2010. Development of subject-
415 specific and statistical shape models of the knee using an efficient segmentation and
416 mesh-morphing approach. Comput. Methods Programs Biomed. 97:232–240.
417 doi:10.1016/j.cmpb.2009.07.005.
418 Carter TE, Taylor KA, Spritzer CE, Utturkar GM, Taylor DC, Moorman CT, Garrett
419 WE, Guilak F, McNulty AL, DeFrate LE. 2015. In vivo cartilage strain increases
420 following medial meniscal tear and correlates with synovial fluid matrix
421 metalloproteinase activity. J. Biomech. 48:1461–1468.
422 doi:10.1016/j.jbiomech.2015.02.030.
423 Danso EK, Mäkelä JTA, Tanska P, Mononen ME, Honkanen JTJ, Jurvelin JS, Töyräs J,
424 Julkunen P, Korhonen RK. 2015. Characterization of site-specific biomechanical
425 properties of human meniscus—Importance of collagen and fluid on mechanical
426 nonlinearities. J. Biomech. 48:1499–1507. doi:10.1016/j.jbiomech.2015.01.048.
427 Dodin P, Pelletier J, Martel-Pelletier J, Abram F. 2010. Automatic Human Knee
428 Cartilage Segmentation From 3-D Magnetic Resonance Images. IEEE Trans. Biomed.
429 Eng. 57:2699–2711. doi:10.1109/TBME.2010.2058112.
430 Elliott DM, Narmoneva DA, Setton LA. 2002. Direct Measurement of the Poisson's
431 Ratio of Human Patella Cartilage in Tension. J. Biomech. Eng. 124:223–228.
432 doi:10.1115/1.1449905.
433 Folkesson J, Dam EB, Olsen OF, Pettersen PC, Christiansen C. 2007. Segmenting
434 Articular Cartilage Automatically Using a Voxel Classification Approach. IEEE Trans.
435 Med. Imaging 26:106–115. doi:10.1109/TMI.2006.886808.
436 Fripp J, Crozier S, Warfield S, Ourselin S. 2007. Automatic segmentation of articular
437 cartilage in magnetic resonance images of the knee. Med. Image Comput. 29:186–194.
438 doi:10.1007/978-3-540-75759-7.
439 Fukubayashi T, Kurosawa H. 1980. The contact area and pressure distribution pattern of
440 the knee. A study of normal and osteoarthrotic knee joints. Acta Orthop. Scand. 51:871–
441 9.
442 Gan H-S, Tan T-S, Wong L-X, Tham W-K, Sayuti KA, Abdul Karim AH, bin Abdul
443 Kadir MR. 2014. Interactive knee cartilage extraction using efficient segmentation
444 software: data from the osteoarthritis initiative. Biomed. Mater. Eng. 24:3145–3157.
445 doi:10.3233/BME-141137.
446 Garcia JJ, Altiero NJ, Haut RC. 1998. An Approach for the Stress Analysis of
447 Transversely Isotropic Biphasic Cartilage Under Impact Load. J. Biomech. Eng.
448 120:608. doi:10.1115/1.2834751.
449 García JJ, Cortés DH. 2007. A biphasic viscohyperelastic fibril-reinforced model for
450 articular cartilage: Formulation and comparison with experimental data. J. Biomech.
451 40:1737–1744. doi:10.1016/j.jbiomech.2006.08.001.
452 Gardiner BS, Woodhouse FG, Besier TF, Grodzinsky AJ, Lloyd DG, Zhang L, Smith
453 DW. 2016. Predicting Knee Osteoarthritis. Ann. Biomed. Eng. 44:222–233.
454 doi:10.1007/s10439-015-1393-5.
455 Goertzen DJ, Budney DR, Cinats JG. 1997. Methodology and apparatus to determine
456 material properties of the knee joint meniscus. Med. Eng. Phys. 19:412–419.
457 doi:10.1016/S1350-4533(97)00011-8.
458 Halonen KS, Mononen ME, Jurvelin JS, Töyräs J, Korhonen RK. 2013. Importance of
459 depth-wise distribution of collagen and proteoglycans in articular cartilage—A 3D finite
460 element study of stresses and strains in human knee joint. J. Biomech. 46:1184–1192.
461 doi:10.1016/j.jbiomech.2012.12.025.

462 Hauch KN, Villegas DF, Haut Donahue TL. 2010. Geometry, time-dependent and
463 failure properties of human meniscal attachments. J. Biomech. 43:463–468.
464 doi:10.1016/j.jbiomech.2009.09.043.
465 Haut Donahue TL, Hull ML, Rashid MM, Jacobs CR. 2003. How the stiffness of
466 meniscal attachments and meniscal material properties affect tibio-femoral contact
467 pressure computed using a validated finite element model of the human knee joint. J.
468 Biomech. 36:19–34. doi:10.1016/S0021-9290(02)00305-6.
469 Kłodowski A, Mononen ME, Kulmala JP, Valkeapää A, Korhonen RK, Avela J,
470 Kiviranta I, Jurvelin JS, Mikkola A. 2015. Merge of motion analysis, multibody
471 dynamics and finite element method for the subject-specific analysis of cartilage
472 loading patterns during gait: differences between rotation and moment-driven models of
473 human knee joint. Multibody Syst. Dyn.:1–20. doi:10.1007/s11044-015-9470-y.
474 Korhonen RK, Wong M, Arokoski J, Lindgren R, Helminen HJ, Hunziker EB, Jurvelin
475 JS. 2002. Importance of the superficial tissue layer for the indentation stiffness of
476 articular cartilage. Med. Eng. Phys. 24:99–108. doi:10.1016/S1350-4533(01)00123-0.
477 Kwon O-R, Kang K-T, Son J, Kwon S-K, Jo S-B, Suh D-S, Choi Y-J, Kim H-J, Koh Y-
478 G. 2014. Biomechanical comparison of fixed- and mobile-bearing for unicomparmental
479 knee arthroplasty using finite element analysis. J. Orthop. Res. 32:338–345.
480 doi:10.1002/jor.22499.
481 Li LP, Buschmann MD, Shirazi-Adl A. 2000. A fibril reinforced nonhomogeneous
482 poroelastic model for articular cartilage: Inhomogeneous response in unconfined
483 compression. J. Biomech. 33:1533–1541. doi:10.1016/S0021-9290(00)00153-6.
484 Li LP, Gu KB. 2011. Reconsideration on the use of elastic models to predict the
485 instantaneous load response of the knee joint. Proceeding Inst. Mech. Eng. 225:888–
486 896. doi:Doi 10.1177/0954411911412464.
487 Mononen ME, Jurvelin JS, Korhonen RK. 2013. Effects of radial tears and partial
488 meniscectomy of lateral meniscus on the knee joint mechanics during the stance phase
489 of the gait cycle - A 3D finite element study. J. Orthop. Res. 31:1208–1217.
490 doi:10.1002/jor.22358.
491 Mononen ME, Tanska P, Isaksson H, Korhonen RK. 2016. A Novel Method to
492 Simulate the Progression of Collagen Degeneration of Cartilage in the Knee : Data from
493 the Osteoarthritis Initiative. Sci. Rep. 6:1–14. doi:10.1038/srep21415.
494 Morimoto Y, Ferretti M, Ekdahl M, Smolinski P, Fu FH. 2009. Tibiofemoral Joint
495 Contact Area and Pressure After Single- and Double-Bundle Anterior Cruciate
496 Ligament Reconstruction. Arthrosc. J. Arthrosc. Relat. Surg. 25:62–69.
497 doi:10.1016/j.arthro.2008.08.014.
498 Mow VC, Gu WY, Chen FH. 2005. Structure and function of articular cartilage and
499 meniscus. In: Mow VC, Huiskes R, editors. Basic Orthopaedic Biomechanics &
500 Mechano-biology. 3rd ed. Philadelphia: Lippincott Williams & Wilkins. p. 181–258.
501 Patil S, Steklov N, Song L, Bae WC, D'Lima DD. 2014. Comparative biomechanical
502 analysis of human and caprine knee articular cartilage. Knee 21:119–125.
503 doi:10.1016/j.knee.2013.03.009.
504 Pedoia V, Majumdar S, Link TM. 2016. Segmentation of joint and musculoskeletal
505 tissue in the study of arthritis. Magn. Reson. Mater. Physics, Biol. Med. 29:207–221.
506 doi:10.1007/s10334-016-0532-9.
507 Shan L, Zach C, Charles C, Niethammer M. 2014. Automatic atlas-based three-label
508 cartilage segmentation from MR knee images. Med. Image Anal. 18:1233–1246.
509 doi:10.1016/j.media.2014.05.008.
510 Shepherd DET, Seedhom BB. 1999. The " instantaneous " compressive modulus of
511 human articular cartilage in joints of the lower limb. Rheumatology 38:124–132.

512 Shim H, Chang S, Tao C, Wang J-H, Kwoh CK, Bae KT. 2009. Knee Cartilage:
513 Efficient and Reproducible Segmentation on High-Spatial-Resolution MR Images with
514 the Semiautomated Graph-Cut Algorithm Method 1. Radiology 251:548–556.
515 doi:10.1148/radiol.2512081332.
516 Tamez-Peña JG, Farber J, González PC, Schreyer E, Schneider E, Totterman S. 2012.
517 Unsupervised segmentation and quantification of anatomical knee features: Data from
518 the osteoarthritis initiative. IEEE Trans. Biomed. Eng. 59:1177–1186.
519 doi:10.1109/TBME.2012.2186612.
520 Vaziri A, Nayeb-Hashemi H, Singh A, Tafti BA. 2008. Influence of Meniscectomy and
521 Meniscus Replacement on the Stress Distribution in Human Knee Joint. Ann. Biomed.
522 Eng. 36:1335–1344. doi:10.1007/s10439-008-9515-y.
523 Velut J, Bolbos R, Beuf O, Odet C, Benoit-Cattin H. 2008. 3-D knee cartilage
524 segmentation using a smoothing B-Spline active surface. In: 2008 15th IEEE
525 International Conference on Image Processing. IEEE. p. 2924–2927.
526 Wilson W, Van Donkelaar CC, Van Rietbergen B, Ito K, Huiskes R. 2004. Stresses in
527 the local collagen network of articular cartilage: A poroviscoelastic fibril-reinforced
528 finite element study. J. Biomech. 37:357–366. doi:10.1016/S0021-9290(03)00267-7.

529

530

Table 1. Subject characteristics.

Geometry	Gender	Age (years)	Height (cm)	Weight (kg)	BMI (kg/m^2)	Laterality
1	Male	27	172	82	25.9	Left
2	Male	28	170	86	29.8	Left
3	Male	30	184	79	23.3	Right
4	Male	26	175	75	24.5	Right
5	Female	26	168	58	20.5	Right
6	Female	70	157	59	23.9	Right

Table 2. Transversely isotropic elastic material parameters for cartilage and meniscus.

Material parameters	Articular cartilage		Meniscus	
E_1, E_2 (MPa)	23.9	(Elliott et al. 2002)	20	(Vaziri et al. 2008)
E_3 (MPa)	8.29	(Shepherd and Seedhom 1999)	159.6	(Mow et al. 2005)
ν_{12}	0.87†	(Elliott et al. 2002)	0.3	(Danso et al. 2015)
ν_{31}	0.15	(Mow et al. 2005)	0.78	(Goertzen et al. 1997)
G_{13} (MPa)	10	(Korhonen et al. 2002)	50	(Vaziri et al. 2008)

$E_1 = E_2$ = in plane Young's modulus, E_3 = out of plane Young's modulus, ν_{12} = in plane Poisson's ratio, ν_{31} = out of plane Poisson's ratio and G_{13} = out of plane shear modulus (see that the planes are different for cartilage and meniscus, Fig. 2)

† in plane Poisson's ratio was obtained from a reference publication (Elliott et al. 2002) but adjusted to fulfil the material stability conditions in Abaqus.

Table 3. Contact pressures, Von Mises stresses and compressive strains (mean ± standard deviation) observed in the models with manually and semi-automatically segmented femoral and tibial cartilages. Results in both manual and semiautomatic cases were calculated using contact areas of the manually segmented geometry.

		Contact Pressure (MPa)		**Von Mises Stress (MPa)**		**Compressive Strain (%)**	
Femur (LAT)	Manual	0.88 ± 0.19	$p = 0.12$	1.22 ± 0.22	$p = 0.92$	5.04 ± 0.78	$p = 0.60$
	Semi	0.67 ± 0.27		1.26 ± 0.32		4.58 ± 1.91	
Femur (MED)	Manual	1.31 ± 0.12	$p = 0.75$	1.54 ± 0.17	$p = 0.12$	7.16 ± 0.40	$p = 0.46$
	Semi	1.27 ± 0.31		1.86 ± 0.36		7.47 ± 1.37	
Tibia (LAT)	Manual	1.16 ± 0.32	$p = 0.046$	1.77 ± 0.45	$p = 0.08$	4.06 ± 0.99	$p = 0.46$
	Semi	0.79 ± 0.35		1.49 ± 0.36		4.41 ± 1.57	
Tibia (MED)	Manual	1.32 ± 1.26	$p = 0.12$	1.81 ± 0.39	$p = 0.75$	4.88 ± 0.82	$p = 0.046$
	Semi	1.76 ± 0.58		2.02 ± 0.6		6.82 ± 2.20	

Semi = semi-automatic, LAT = lateral, MED = medial. Statistical analysis was conducted using Wilcoxon signed-rank test.

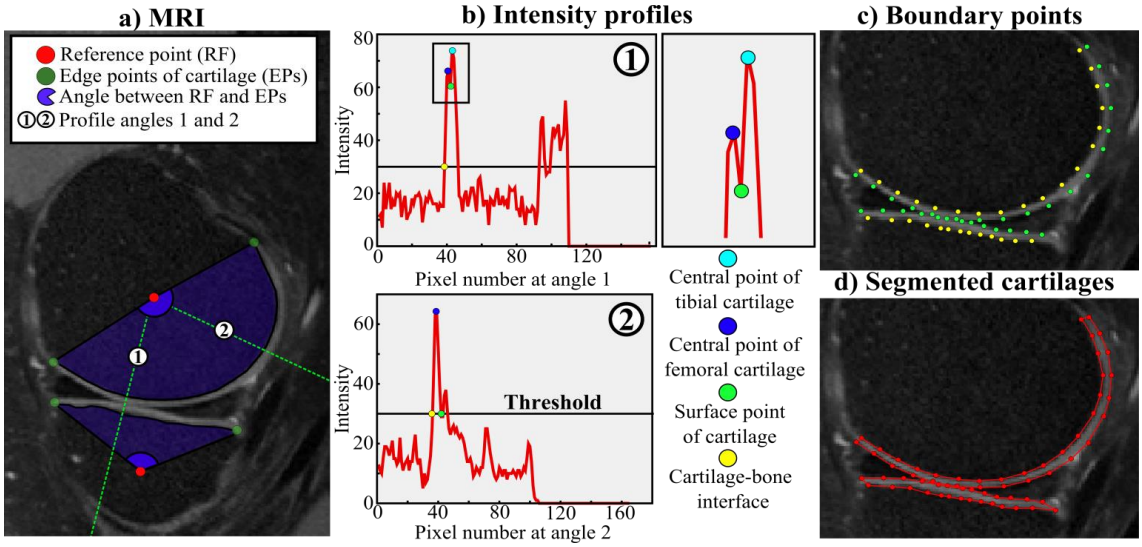

548

549 Figure 1. Segmentation method based on radial intensity profiles. a) An example
550 demonstrating how to select reference points and edge points of femoral and tibial
551 cartilage from an MRI slice. b) Typical intensity profiles from (1) and (2). Central
552 points of tibial and femoral cartilage, cartilage surface and bone-cartilage interface are
553 marked by cyan, blue, green and yellow, respectively. Threshold values were chosen
554 based on the intensity profiles (see more details in the text). c) Cartilage-bone interface
555 and cartilage surface observed from every intensity profile in tibial and femoral
556 cartilage. d) Final segmentations for femoral and tibial cartilages.
557

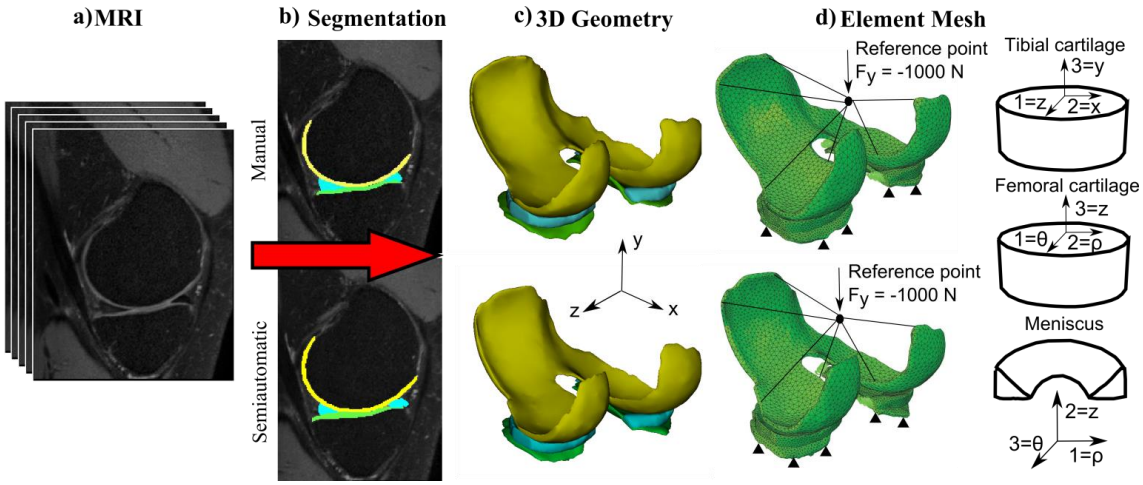

558

559 Figure 2. a) Magnetic resonance images were segmented using both b) manual and
560 semi-automatic segmentation methods. Then, c) from constructed 3D geometries d)
561 tetrahedral element meshes were generated. Finally, d) boundary conditions, axial
562 impact loads and transverse isotropic material properties were implemented into the

knee joint FE models. In the tibial cartilage, a cartesian coordinate system was applied, whereas in the femoral cartilage and menisci, cylinder coordinate systems were applied. Note that the plane of isotropy was 1-2 for all tissues, but this plane is not the same for cartilage and meniscus (see Table 2).

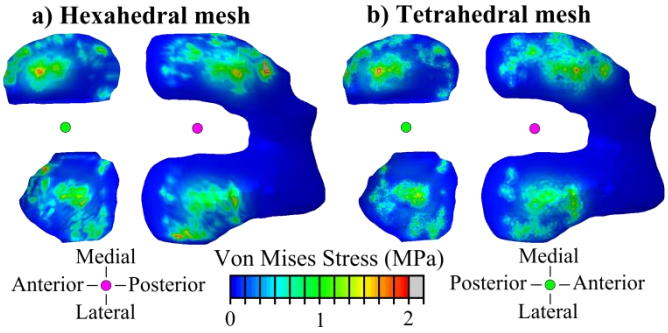

Figure 3. A mesh sensitivity study was conducted by comparing the hexahedral (a) and tetrahedral (b) meshes. A tetrahedral mesh (b) was considered to be adequate for these simulations since differences in Von Mises stresses and compressive strains between the whole knee joint models were small (4.4 % and 8.2 %, respectively).

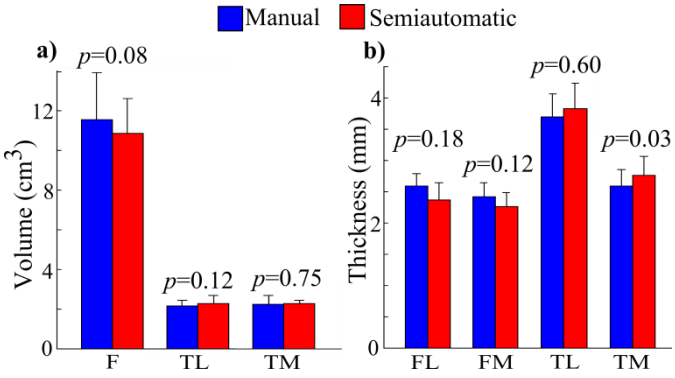

Figure 4. a) Volumes and b) thicknesses (mean ± standard deviation) of tibial and femoral cartilages. Thicknesses in both manual and semi-automatic cases were calculated from the contact area of manually segmented cartilage. F = femoral cartilage, T = tibial cartilage, L = lateral, M = medial. Wilcoxon signed-rank test was used for statistical comparisons.

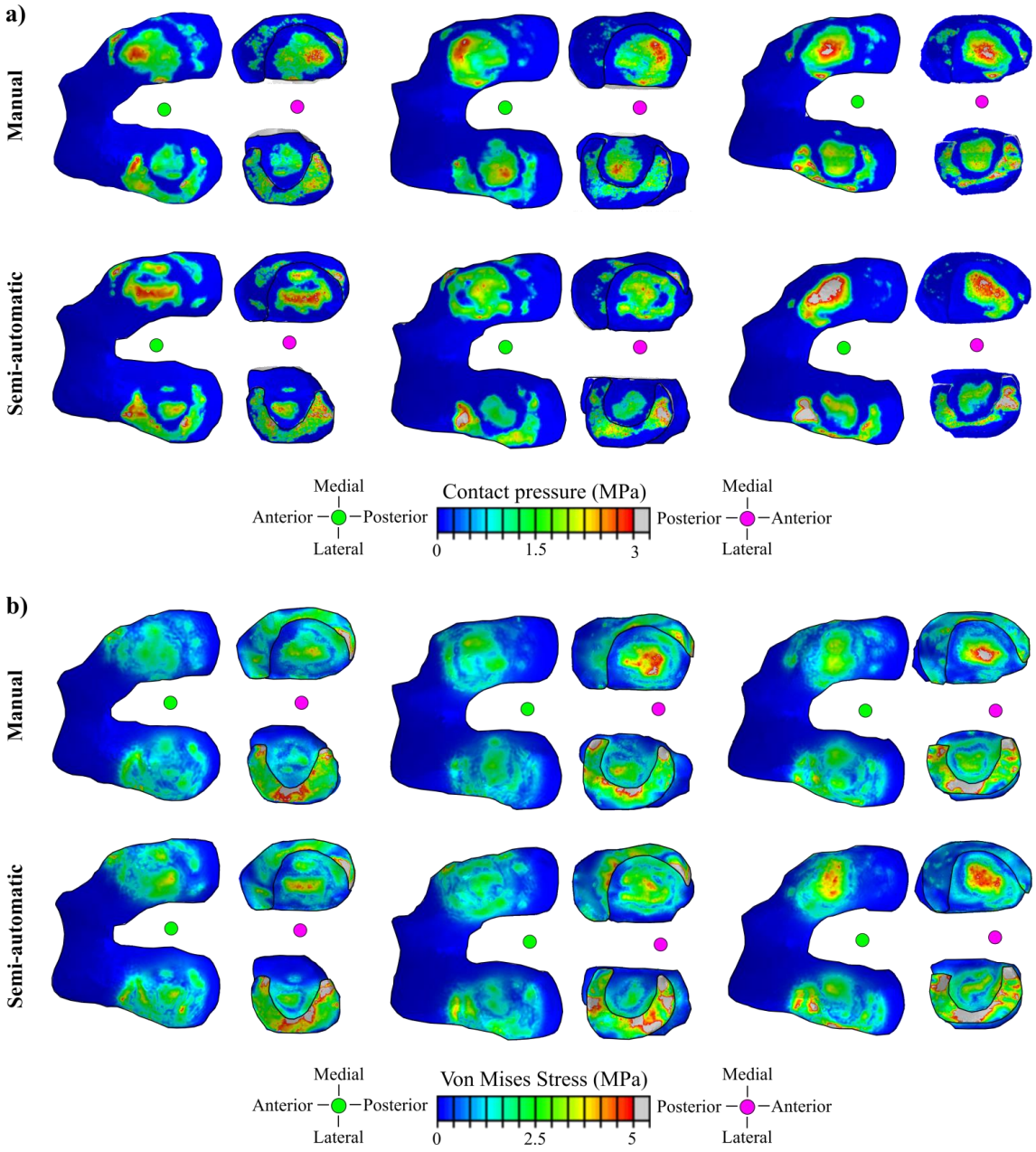

581

582 Figure 5. a) Contact pressure and b) Von Mises stress distributions of three different
583 knee joint models with manually and semi-automatically segmented geometries.
584

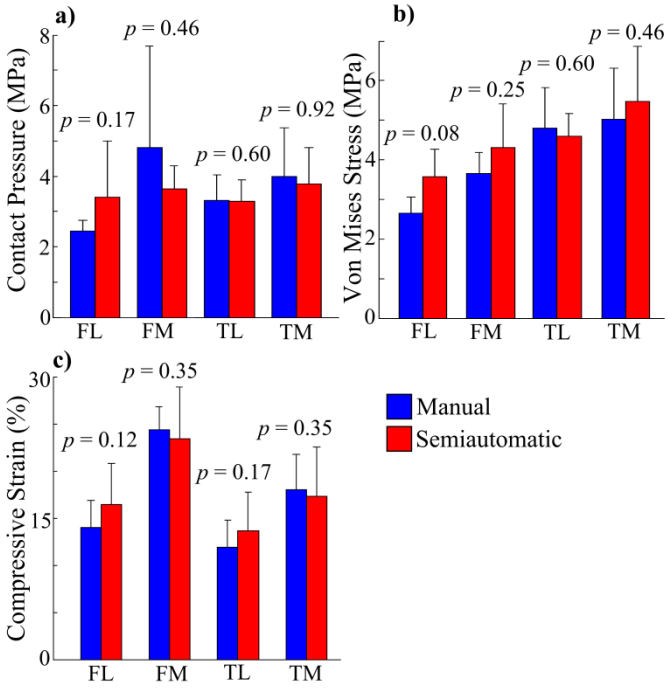

585

586 Figure 6. Statistical comparison of maximum values (mean ± standard deviation) of a)
587 contact pressures, b) Von Mises stresses, and c) compressive strains observed in the
588 models with manually and semi-automatically segmented femoral and tibial cartilages.
589 F = femoral cartilage, T = tibial cartilage, L = lateral, M = medial. Wilcoxon signed-
590 rank test was used for statistical comparisons.

591

592 **Supplementary material**

593

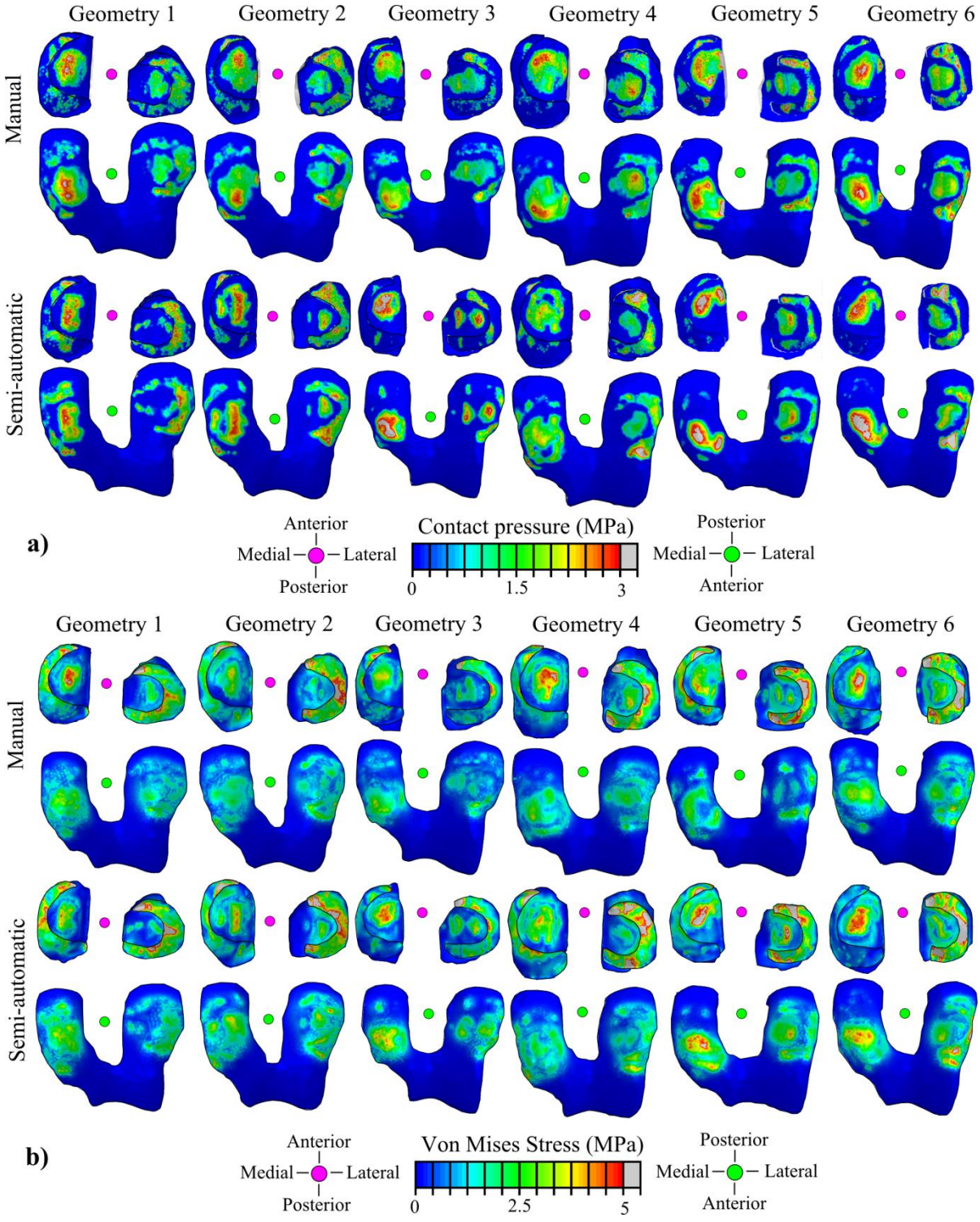

594

595 Fig 1. a) Contact pressure and b) Von Mises stress distributions of all the knee joint models with
596 manually and semiautomatically segmented geometries.

597